

# Pore Pressure Response Following Undrained uCPT Sounding in a Dilating Soil

Derek Elsworth<sup>1</sup>; Dae Sung Lee<sup>2</sup>; Roman Hryciw<sup>3</sup>; and Seungcheol Shin<sup>4</sup>

**Abstract:** The generation and dissipation of pore fluid pressures following standard piezocone sounding (uCPT) sounding in silty sands are observed to exhibit many of the characteristics of undrained penetration in dilatant materials; steady excess pore pressures may be subhydrostatic, or may become subhydrostatic during dissipation, and are slow to decay. Enigmatic pore pressure dissipation histories which transit from sub- to supra- and again to subhydrostatic before equilibrating at hydrostatic are consistent with a response where undrained pressures are maximally negative remote from the penetrometer tip. This surprising distribution of induced pore fluid pressures is accommodated in cavity expansion models for a dilating soil. A Mohr-Coulomb constitutive model is established for undrained loading of a soil with pore pressure response defined by Skempton pore pressure parameters. Defined in terms of effective stresses, this allows undrained stresses and pore pressures to be determined following cavity expansion in a  $c-\phi$  soil. Pore pressures are conditioned by the shear modulus, Skempton  $A$  parameter, and the “undrained shear strength.” The undrained shear strength is additionally modulated by the magnitudes of  $c$ ,  $\phi$ ,  $A$ , and of the initial in situ effective stress,  $\sigma'_0$ . Cavity expansion stresses, and pore pressures may be backcalculated. Undrained pore pressures are shown to decay loglinearly with radius from the cavity wall; they may be either supra- or subhydrostatic at the cavity wall, and where suprahydrostatic may become subhydrostatic close to the transition to the elastic region. This initial pressure distribution contributes to the observed switching between supra- and subhydrostatic pore pressures recorded during dissipation. “Type curves” that reflect the dissipation response enable the consolidation coefficient, undrained strength, and shear modulus to be computed from observed pore pressure data, and confirmed against independent measurements. In addition to representing the dilatatory response of cohesionless silts, the method applies equally to recovering the pressure generation and dissipation response of overconsolidated clays.

**DOI:** 10.1061/(ASCE)1090-0241(2006)132:11(1485)

**CE Database subject headings:** Cone penetration tests; Constitutive relations; Dilatancy; Overconsolidated soils; Pore water pressure; Poroelasticity.

## Introduction

Piezocone sounding (uCPT) is an evolving rapid, minimally invasive and inexpensive method for determining the mechanical and transport properties of soil, their spatial distribution, and the type and distribution of the soil-saturants (Campanella and Robertson 1988; Mitchell and Brandon 1998). Indirect methods to determine the transport characteristics of soils alternately rely on empirical correlations with soil gradation (Douglas and Olsen 1981; Manassero 1994; Robertson et al. 1986), from the imaging

of soil fabric (Hryciw et al. 2003), or from correlations with cone metrics (Chiang et al. 1992; Smythe et al. 1989). Direct measurements may also be made using direct-push permeameters (Auxt and Wright 1995; Konrad and Frechette 1995; Lowry 1998; Scaturro and Wissowson 1997), or by measuring either rates of dissipation of excess pore pressures (Burns and Mayne 1998; Elsworth 1993; Gribb et al. 1998; Lunne et al. 1997; Robertson et al. 1992; Schmertmann 1978; Teh and Houlsby 1991; Torstensson 1977) or their on-the-fly magnitudes (Elsworth 1993; Elsworth 1998; Elsworth and Lee 2006; Voyiadjis and Song 2003). Importantly, dissipation tests are usually conducted following undrained penetration where the dissipation of pore pressures following cone arrest are controlled by the coefficient of consolidation alone—additional assumptions regarding soil compressibility are required to allow estimation of the coefficient of permeability. Conversely, on-the-fly pressure tests require that the loading is only partially drained, and consequently allow on-the-fly pressures to be a direct index of permeability.

Dissipation behavior is typically discussed in relation to penetration in clays. The development of undrained pore pressures is typically evaluated using cavity expansion (Burns and Mayne 1998; Torstensson 1977) or strain path models (Baligh 1985; Baligh and Levadoux 1986; Danziger et al. 1997; Levadoux and Baligh 1986; Teh and Houlsby 1991) to define initial pore pressure distributions that subsequently dissipate to background levels. These evaluations compare well with field (Baligh and Levadoux 1986; Levadoux and Baligh 1986) and calibration chamber (Kurup et al. 1994) results. Predictions from complex

<sup>1</sup>Dept. of Energy and Geo-Environmental Engineering and the Energy Institute, Pennsylvania State Univ., University Park, PA 16802-5000. E-mail: elsworth@psu.edu

<sup>2</sup>Dept. of Energy and Geo-Environmental Engineering and the Energy Institute, Pennsylvania State Univ., University Park, PA 16802-5000. E-mail: leethumb@psu.edu

<sup>3</sup>Dept. of Civil and Environmental Engineering, Univ. of Michigan, Ann Arbor, MI 48109-2125. E-mail: romanh@umich.edu

<sup>4</sup>Dept. of Civil and Environmental Engineering, Univ. of Michigan, Ann Arbor, MI 48109-2125. E-mail: shinsc@umich.edu

Note. Discussion open until April 1, 2007. Separate discussions must be submitted for individual papers. To extend the closing date by one month, a written request must be filed with the ASCE Managing Editor. The manuscript for this paper was submitted for review and possible publication on September 27, 2005; approved on April 29, 2006. This paper is part of the *Journal of Geotechnical and Geoenvironmental Engineering*, Vol. 132, No. 11, November 1, 2006. ©ASCE, ISSN 1090-0241/2006/11-1485-1495/\$25.00.

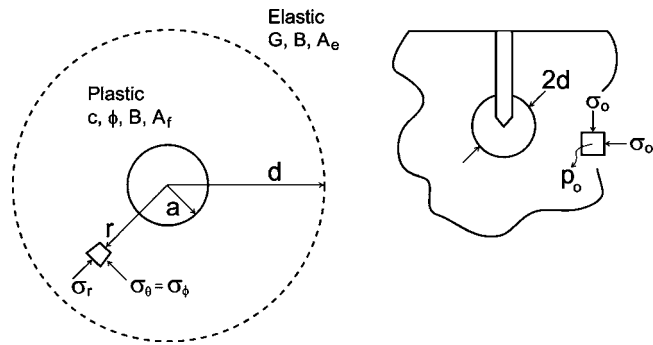


Fig. 1. Spherical geometry of cavity inflated within an infinite medium

(Baligh and Levadoux 1986) and simple material models (Teh and Houlsby 1991) compare well with more rigorous representations of finite strain continuum behavior for clays (Kiousis and Voyiadjis 1985; Voyiadjis and Abu-Farsakh 1997; Voyiadjis and Song 2000), sands (Cividini and Gioda 1988), and clays to sands (Van den Berg 1994). For linear soil behavior, a variant of these methods may be applied to account for partial drainage in an effective stress analysis (Elsworth 1991, 1993, 1998) and this yields similar results to those from strain path and continuum models.

Although able to accommodate various soil models including overconsolidated and dilatant clays (Burns and Mayne 1998; Levadoux and Baligh 1986), undrained and dilatant response should not be restricted to penetration in cohesive materials. Recent observations of pressure dissipation following arrested penetration in silty sands exhibit many of the attributes of undrained penetration in dilatant soils. A mechanistic model to describe this observed response is examined in the following.

## Mechanical Response

We examine the mechanical response adjacent to the undrained expansion of a spherical cavity in a dilating soil, as a model for the local response to penetrometer insertion. The cavity is of radius  $a$ , within a soil subject to uniform initial total stress of  $\sigma_0$  and initial pore pressure  $p_0$ . This geometry is illustrated in Fig. 1. Equilibrium of total stresses is enforced for the assumed spherically symmetric geometry, accommodating Mohr-Coulomb failure and absent of any change in volume. This enables the instantaneous undrained pore pressure distribution to be defined adjacent to the cavity.

## Undrained Pore Pressures

Pore pressure change  $\delta p$  generated by changes in total maximum  $\delta\sigma_1$  and minimum  $\delta\sigma_3$  principal stresses may be determined in terms of the pore pressure coefficients  $A$  and  $B$  (Skempton 1954) as

$$\delta p = B\delta\sigma_3 + BA(\delta\sigma_1 - \delta\sigma_3) \quad (1)$$

The change in pore pressure is relative to an initial static pore pressure of magnitude  $p_0$  and the change in the intermediate principal stress  $\delta\sigma_2$  follows the minimum principal stress as  $\delta\sigma_2 = \delta\sigma_3$ . Final stress ( $\sigma_1, \sigma_3$ ) and pore pressure  $p$  magnitudes are defined relative to initial magnitudes of the isotropic total stress ( $\sigma_0$ ) and initial pore pressure ( $p_0$ ) as

$$\sigma_1 = \sigma_0 + \delta\sigma_1 \quad (2)$$

$$\sigma_3 = \sigma_0 + \delta\sigma_3 \quad (3)$$

$$p = p_0 + \delta p \quad (4)$$

with compressive stresses and pore fluid pressures defined positive. Substituting Eqs. (2)–(4) into Eq. (1) enables generated pore pressures to be defined in terms of final total stresses as

$$p = (p_0 - B\sigma_0) + B\sigma_3 + BA(\sigma_1 - \sigma_3) \quad (5)$$

This defines the resulting pore fluid pressure relative to the induced total stresses that will be used in solving the stress equilibrium equation.

## Constitutive Behavior

The Mohr-Coulomb criterion may be defined in terms of maximum  $\sigma'_1$  and minimum  $\sigma'_3$  principal effective stresses as

$$\sigma'_1 = N\sigma'_3 + 2c\sqrt{N} \quad (6)$$

where  $c$  = cohesion and  $N$  indexes the frictional strength in terms of the frictional coefficient  $\phi'$  as  $N = (1 + \sin \phi') / (1 - \sin \phi')$ . Effective stresses are defined as  $\sigma'_i = \sigma_i - \alpha p$ , where the Biot coefficient  $\alpha$  is approximated as unity. Substituting for effective stresses in the failure criterion of Eq. (6) gives strength in terms of total stresses as

$$\sigma_1 = N\sigma_3 + (1 - N)p + 2c\sqrt{N} \quad (7)$$

The undrained pore pressures of Eq. (5) may be substituted into Eq. (7) to yield the strength criterion defined in terms of total stresses as

$$\sigma_1 = \frac{[N + (1 - N)(1 - A)B]}{[1 - (1 - N)BA]} \sigma_3 + \frac{[N - 1](B\sigma_0 - p_0) + 2c\sqrt{N}}{[1 - (1 - N)BA]} \quad (8)$$

Importantly, this strength criterion defines an effective cohesion in the second term on the right-hand side that includes two components. The first is due to the frictional resistance acting via the assumed uniform initial in situ effective stress ( $B\sigma_0 - p_0$ ), which is independent of stress change and invariant in space and time, and the second is a true cohesive component present when  $c \neq 0$ . Most transparently, when  $B = 1$ , the bracketed first term on the right-hand side of Eq. (8) reduces to unity, and the expression is redefined as

$$\sigma_1 = \sigma_3 + 2\zeta \quad (9)$$

where

$$2\zeta = \frac{[N - 1]\sigma'_0 + 2c\sqrt{N}}{[1 - (1 - N)A]} \quad (10)$$

Notably, the new strength criterion of Eq. (9) is in the form of a Tresca criterion. In this the shear strength ( $\sigma_1 - \sigma_3$ ) is not dependent on the minimum principal stress  $\sigma_3$ , and can be effectively represented by an effective undrained strength of  $\zeta = S_u$ . Note that a distinction is made between the initial cohesive strength of the soil ( $c \neq 0$ ), such as due to an initial adhesion between soil grains, that may be destroyed by large displacements in the tip-local process zone, and the resulting undrained strength that results from the frictional contribution via changes in undrained pore pressures ( $\zeta = S_u \neq 0$ ). The adhesion is a microscopic property, whereas the

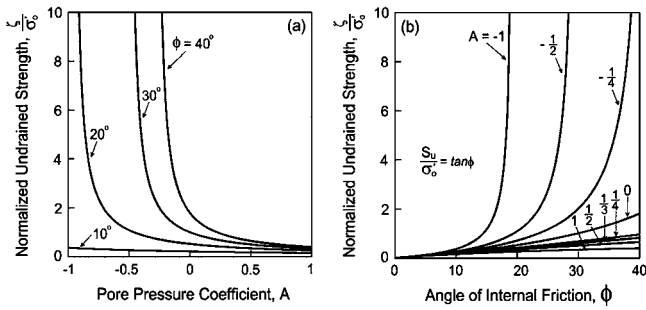


Fig. 2. Variation of normalized undrained strength with (a) Skempton pore pressure coefficient  $A$ ; (b) angle of internal friction

undrained strength is a macroscopic property of strength, which in this case replaces the frictional strength.

The principal assumption embodied in Eqs. (9) and (10) is that loading is undrained. This condition is met if the permeability is sufficiently small, relative to the loading or soil strain (dilation or compaction) rate—a condition that is typically satisfied for uCPT sounding in clays and silts, and even in fine sands. This ratio of pressure generation and pressure loss can be indexed relative to either material properties, or to cone measured indices. To first order, penetration response transits to undrained where the dimensionless permeability,  $K_D = (4K\sigma'_0)/(Ua\gamma_w)$  is less than unity ( $K_D < 1$ ), as defined through permeability of the penetrated soil,  $K$ , the initial effective stress,  $\sigma'_0$ , penetration rate,  $U$ , penetrometer radius,  $a$ , and the unit weight of water,  $\gamma_w$  (Elsworth and Lee 2005, 2006). Nondimensional permeability  $K_D$  represents the ratio of the rate of dissipation of fluid mass from the tip-local zone, to the rate of pressure generation by either dilation or compaction. The reciprocal of dimensionless permeability ( $K_D = 1/B_qQ_t$ ) is alternately represented by the ensemble cone index of the product of penetration measured pore pressure ratio ( $B_q$ ) and end bearing ( $Q_t$ ). Penetration is undrained when the product  $B_qQ_t$  is greater than about unity ( $B_qQ_t > 1$ ). Additionally, undrained loading absent the escape of fluid mass infers no net volume change in the soil-water assemblage, allowing simplified treatment of postfailure behavior in plasticity models.

Where displacements are sufficiently large to destroy any initial cohesion, or where frictional strength dominates, the failure criterion of Eq. (10), reduces to

$$2\zeta = \frac{[N-1]}{[1-(1-N)A]}\sigma'_0 \quad (11)$$

In this instance, the undrained strength  $\zeta = S_u$  is controlled by the angle of internal friction  $\phi'$ , the pore pressure coefficient  $A$  and the initial uniform in situ effective stress  $\sigma'_0$ , only. The variation of “normalized undrained strength”  $\zeta/\sigma'_0 \equiv S_u/\sigma'_0$  with  $A$  for  $10^\circ < \phi' < 40^\circ$  is shown in Fig. 2(a). It is always positive and nonzero, with a singular magnitude at  $A = 1/(1-N)$ .

The “undrained strength”  $\zeta$  may be considered analogous to the effective frictional strength modulated by in situ effective stress as  $\zeta = S_u = \sigma'_0 \tan \phi$ , as utilized to describe the rigidity index in terms of the shear modulus  $G$  as  $G/S_u = G/(c + \sigma'_0 \tan \phi)$  (Vesic 1972). Thus where cohesion is negligible, the resulting drained ( $S_u/\sigma'_0 = \tan \phi$ ) and undrained ( $\zeta/\sigma'_0 = \frac{1}{2}[N-1]/[1-(1-N)A]$ ; from Eq. (11)) strength ratios may be compared for various magnitudes of the pore pressure parameter  $A$  as in Fig. 2(b). The strength ratios  $S_u/\sigma'_0$  and  $\zeta/\sigma'_0$  are identical when  $A = \frac{1}{3}$ , corresponding to the elastic magnitude of  $A$ . As the pore pressure

coefficient is increased relative to this, the material becomes weaker as excess pore pressures reduce the effective stresses. Conversely, for  $A < \frac{1}{3}$  the undrained strength is increased as a consequence of dilatancy.

### Stress Distribution around a Spherical Cavity

We describe the expansion of a spherical cavity within a soil where strength is independent of the local mean stress magnitude as  $\sigma_1 = \sigma_3 + 2\zeta$ , and where failure evolves absent volume change. This solution is directly analogous to cavity expansion within an elastic-perfectly plastic soil with equivalent shear modulus  $G$  and undrained shear strength  $S_u = \zeta$ . Satisfying equilibrium between radial  $\sigma_r$  and tangential  $\sigma_\theta$  total stresses everywhere (Fig. 1) as  $d\sigma_r/dr + 2(\sigma_r - \sigma_\theta)/r = 0$ , subject to the strength criterion  $\sigma_1 = \sigma_3 + 2\zeta$  in the failed zone, and Hooke's law in the elastic region, yields changes in the radial ( $\delta\sigma_r = \delta\sigma_1$ ) and tangential ( $\delta\sigma_\theta = \delta\sigma_3$ ) stresses in the failed region as (Elsworth and Lee 2006; Hill 1983)

$$\delta\sigma_r = \frac{4}{3}\zeta[1 + \ln(G/\zeta) + 3 \ln(ar)] \quad (12)$$

$$\delta\sigma_\theta = \frac{4}{3}\zeta[-\frac{1}{2} + \ln(G/\zeta) + 3 \ln(ar)] \quad (13)$$

The failed zone extends to a radial distance  $d = a(G/\zeta)^{1/3}$  around the cavity of radius  $r = a$ , with the change in radial stress at distance  $d$  obtained by setting  $r = a(G/\zeta)^{1/3}$  in Eq. (12) to yield  $\delta\sigma_r|_{r=d} = \frac{4}{3}\zeta$ . Beyond this radius, the changes in stresses are elastic and are defined by the Lamé relations (Hill 1983), where substituting  $\delta\sigma_r|_{r=d} = \frac{4}{3}\zeta$  and  $d = a(G/\zeta)^{1/3}$  yields

$$\delta\sigma_r = \delta\sigma_r|_{r=d} \frac{d^3}{r^3} = \frac{4}{3}G \frac{a^3}{r^3} \quad (14)$$

$$\delta\sigma_\theta = -\frac{1}{2}\delta\sigma_r|_{r=d} \frac{d^3}{r^3} = -\frac{2}{3}G \frac{a^3}{r^3} \quad (15)$$

These provide the necessary relations to define initial undrained pore pressures.

### Undrained Pore Pressure Distribution

With undrained changes in total stresses defined for both the failed [Eqs. (12) and (13)] and elastic [Eqs. (14) and (15)] regions, the resulting changes in pore fluid pressures may also be defined. Where a distinction is made between the pore pressure parameters of the failed ( $B=1; A=A_f$ ) and elastic ( $B=1; A=A_e = \frac{1}{3}$ ) (Elsworth 1991) regions, the resulting pore pressure distributions may be determined. For the failed region ( $a < r < a(G/\zeta)^{1/3}$ ), the undrained pore pressure change is defined by substituting Eqs. (12) and (13) into Eq. (1) as

$$\delta p = p - p_0 = \frac{4}{3}\zeta[(1 + \ln(G/\zeta)) - \frac{3}{2}(1 - A_f) + 3 \ln(ar)] \quad (16)$$

For the elastic region ( $a(G/\zeta)^{1/3} < r < \infty$ ) the pore pressures are similarly evaluated by substituting Eqs. (14) and (15) into Eq. (1) to yield a null change in pore pressure as  $\delta p = 0$ . This null change in pore pressure results since the change in mean stress in the elastic zone is zero and any resulting deviatoric loading results in null volume change, and therefore no change in pressure.

These results are similar to those defined for undrained expansion of a cylindrical cavity in clays where induced pore pressures are indexed to the mean stress (Randolph and Wroth 1979), or for cylindrical and spherical geometries where induced pore pres-

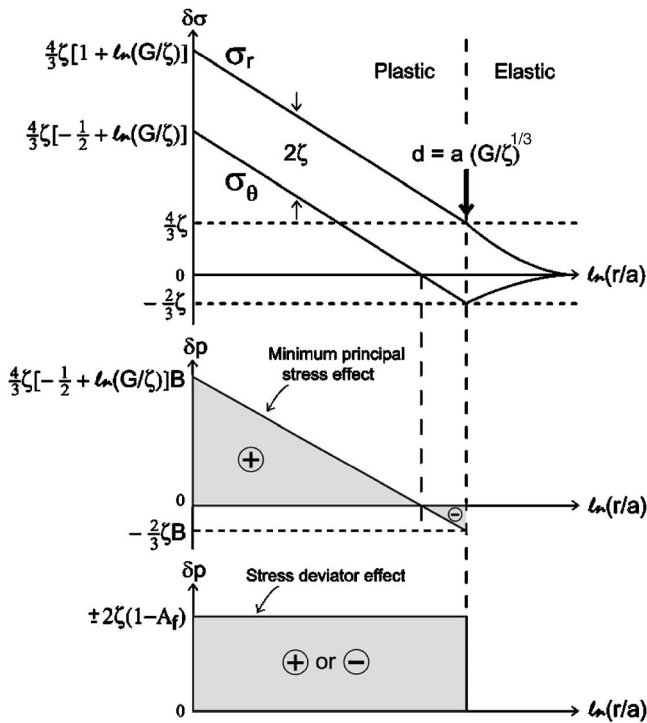


**Fig. 3.** Variation in induced stresses and pore fluid pressures with radius from the wall of an expanded cavity within a saturated medium ( $B=1$ )

ures are determined from Skempton's pore pressure coefficients (Battaglio et al. 1981). However, the constraint of applying only to cohesive soils is now lifted. As in other representations of cavity expansion in granular material, the limit stress is modulated by the shear modulus (Vesic 1972), although now the influence of undrained pore fluid pressures is directly incorporated.

The resulting changes in total stresses and in pore fluid pressures are illustrated schematically in Fig. 3. In the failed zone, the stress difference is given by  $\delta\sigma_r - \delta\sigma_\theta = \sigma_r - \sigma_\theta = 2\zeta$ , and is constant throughout, whereas both the minimum and maximum principal stresses decrease linearly with log radius. Correspondingly, pore pressures induced by the stress difference are uniform throughout the failed zone, and may be either positive or negative, depending on the pore pressure coefficients. Undrained pore pressure changes modulated by the minimum principal stress decrease log-linearly with radius from their peak at the cavity surface, with the potential to become negative at the interface with the elastic zone. The ultimate pressure change distribution is the combination of these effects, resulting in a pressure dropping monotonically with log radius.

The resulting normalized undrained pore pressures are uniquely defined by the coefficients  $\delta p/\zeta = \mathcal{J}[G/\zeta; A_f; r/a]$ , where  $\zeta$  is a unique function of pore pressure coefficient  $A_f$ , friction angle  $\phi'$ , and initial mean stress  $\sigma_0$ . Although coefficients  $\zeta$  and  $A_f$ , and perhaps  $\zeta$  and  $G$ , are related, it is instructive to consider the anticipated influence of  $G/\zeta$  and  $A_f$  on the anticipated radial distribution of change in normalized pore pressures  $\delta p/\zeta$  with normalized radius  $r/a$ , as illustrated in Fig. 4. These illustrate that normalized excess pore pressures increase with an increase in either of the parameters  $A_f$  or  $G/\zeta$ . The pore pressure distribution is discontinuous, as is the change in tangential total stress, although radial total stresses are continuous. The abrupt transition

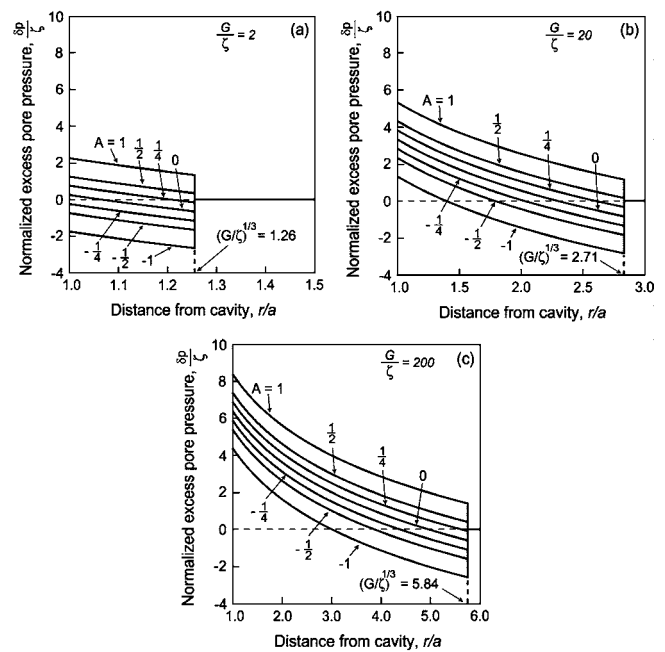


**Fig. 4.** Variation in normalized excess pore pressure with dimensionless radius for ratios of shear modulus to undrained strength ( $G/\zeta$ ) of (a) 2; (b) 20; and (c) 200

of both pore pressures and tangential stresses at the outermost boundary of the plastic zone is a characteristic of the assumption of elastic-perfectly plastic constitutive behavior.

### Pressure Dissipation Response

With the undrained pressure distribution defined with radius, the dissipation response may be determined. Subject to appropriate magnitudes of the controlling parameters, the dissipation response may be described by a set of "type curves," to enable transport parameters to be recovered from the pressure dissipation data.

### Pressure Diffusion Equation

The dissipation response may be described relative to the spherical symmetry of the problem geometry through the diffusion equation

$$\kappa \left[ \frac{\partial^2 p}{\partial r^2} + \frac{2}{r} \frac{\partial p}{\partial r} \right] = \frac{\partial p}{\partial t} \quad (17)$$

defining changes in pressure  $p$  with time  $t$ , as modulated by hydraulic diffusivity or analogous consolidation coefficient  $\kappa$ . Initial conditions for the uncoupled analysis are defined in terms of fluid pressures relative to the baseline background pressure  $p_0$  (Fig. 1). These initial excess pressures are defined within the failed region  $a < r < a(G/\zeta)^{1/3}$  by Eq. (16), and are null within the elastic region  $a(G/\zeta)^{1/3} < r < \infty$ . These initial conditions are supplemented by boundary conditions  $\partial p/\partial r = 0$  at  $r = a$ , and  $p = p_0$  at  $r = \infty$ . These conditions are applied to solve Eq. (17) using an axisymmetric finite element approximation. Variation within individual three-noded elements is linear, and the solution in time is by forward differencing (implicit method). The rectangular mesh extends to 20 cavity radii above, below, and to the side of the cavity, with a total of 24,000 degrees of freedom. The consolidation co-

efficient  $\kappa$  is prescribed uniform in space, and constant in time, with the solution proceeding at logarithmically varying time steps to a maximum nondimensional time of  $t_D = \kappa t/a^2 = 10^2$ .

### Type Curves

The pore pressure response may be defined most conveniently where Eq. (17) is recast in nondimensional form as

$$\left[ \frac{\partial^2 P_D}{\partial r_D^2} + \frac{2}{r_D} \frac{\partial P_D}{\partial r_D} \right] = \frac{\partial P_D}{\partial t_D} \quad (18)$$

where nondimensional pressure  $P_D = (p - p_0)/\zeta$  varies in space  $r_D = r/a$  and time  $t_D = \kappa t/a^2$ . Similar to Eq. (17), initial conditions are for  $P_D = 0$  at  $t_D = 0$ , and boundary conditions are  $\partial P_D / \partial r_D = 0$  at  $r_D = 1$ , and  $P_D = 0$  at  $r_D = \infty$ . In turn, nondimensional pressures are indexed to the undrained response as  $\delta p/\zeta = \mathfrak{J}[G/\zeta; A_f; r_D]$  with the parameter  $\zeta$  additionally modulated by  $\zeta = \mathfrak{J}[N; A_f; \sigma'_0; \text{and } c]$ . Correspondingly, the two parameters of nondimensional pressure  $P_D$  and time  $t_D$  are sufficient to examine the evolution of pressure measured at the cone face,  $r_D = 1$ .

At the cavity face ( $r_D = 1$ ) the dissipation response ( $P_D; t_D$ ) may be represented uniquely for the two parameters of shear modulus to strength ratio  $G/\zeta$  and Skempton pore pressure parameter  $A_f$ . The dissipation response is shown for three representative magnitudes of  $G/\zeta = 2, 20$ , and 200 and for pore pressure coefficients in the range  $-1 < A_f < 1$  in Fig. 5. Where  $G/\zeta$  is smallest, the magnitude of the initial pore pressure distribution is also the smallest magnitude [Fig. 4(a)], and results in the shortest time history for pressures to decay [Fig. 5(a)]. Both pore pressure magnitude and time-to-decay increase as  $G/\zeta$  increases. As the magnitude of  $A_f$  decreases, both the magnitudes of the initial undrained pressures decrease, and the potential to develop negative pore pressures away from the cavity increases. Correspondingly, for intermediate and small (negative) magnitudes of  $A_f$ , pore pressures at the cavity face may begin positive, but become negative once negative pressures that are developed further into the failed zone reverse-diffuse towards the cavity. This feature is apparent for all selected shear moduli  $G/\zeta$  but the threshold to this behavior occurs at progressively smaller magnitudes of the pore pressure parameter  $A_f$  as  $G/\zeta$  increases. Where initial undrained pore pressures at the cavity face are subhydrostatic (e.g., Figs. 4(a) and 5(a);  $A_f < -1/4$ ), then pore pressures remain negative throughout the pressure history. Ultimately the pressure record dissipates to background levels (i.e.,  $P_D = 0$ ) and is of the order of 95% complete at  $t_D > 10^0$ .

Type curves may be directly compared with field data to determine the in situ material parameters affecting the undrained pore pressure and strength response ( $\zeta$ ), and of transport parameters ( $\kappa$ ). In matching with field data, it is convenient to compare the absolute magnitudes of log-pressure with log-time, as represented in Fig. 6. These are merely replots of the responses shown in Fig. 5, with negative pressures shown as their absolute value (i.e., as positive to allow them to be shown on a log-log plot).

### Data Analysis

A series of uCPT dissipation tests were conducted in silty sands near Milan, Mich. These tests involved standard penetration at 2 cm/s using a standard 60° cone of 10 cm<sup>2</sup> end-bearing area. Pore pressures recorded during steady penetration were typically subhydrostatic but upon cone arrest would first become suprah-

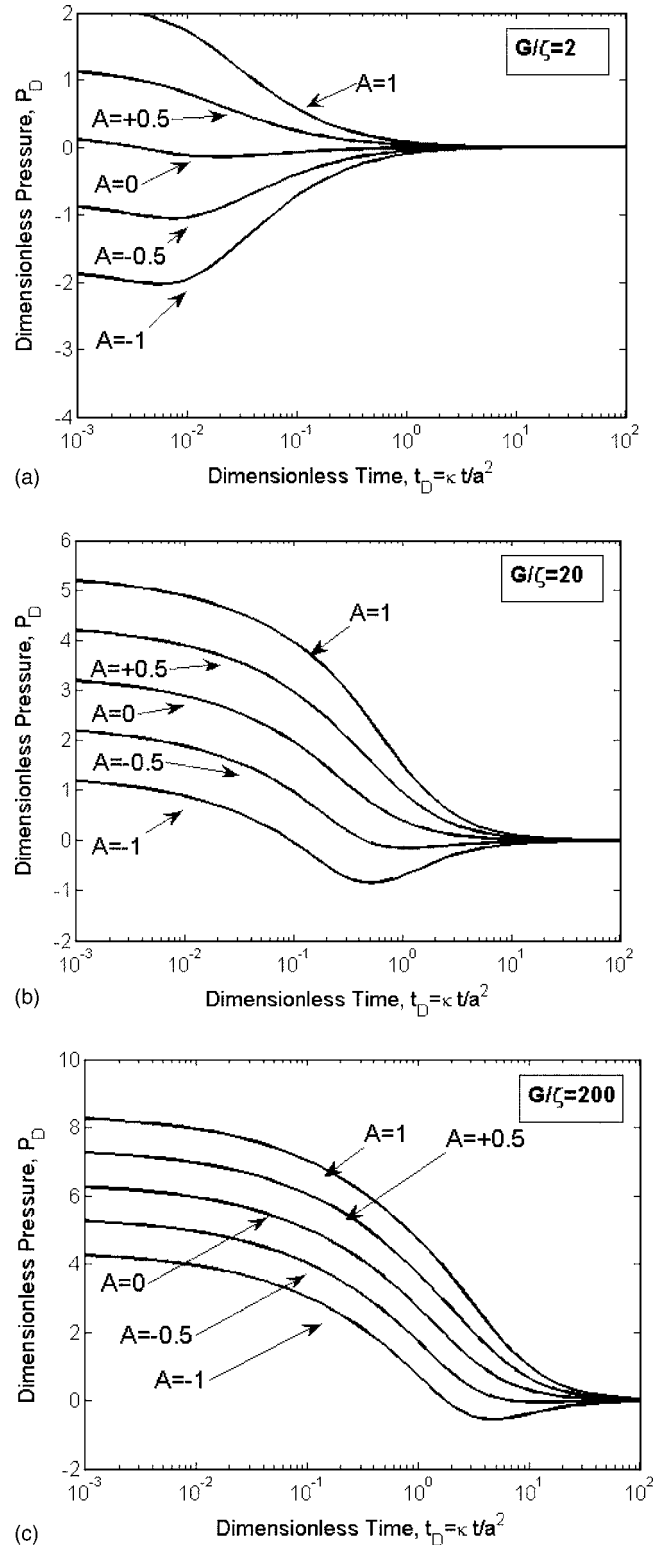
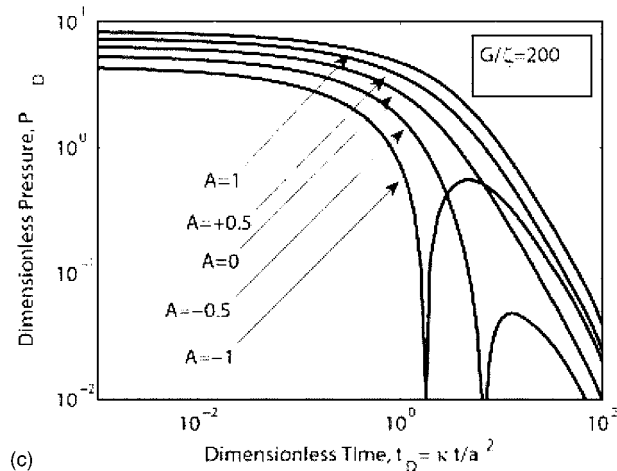
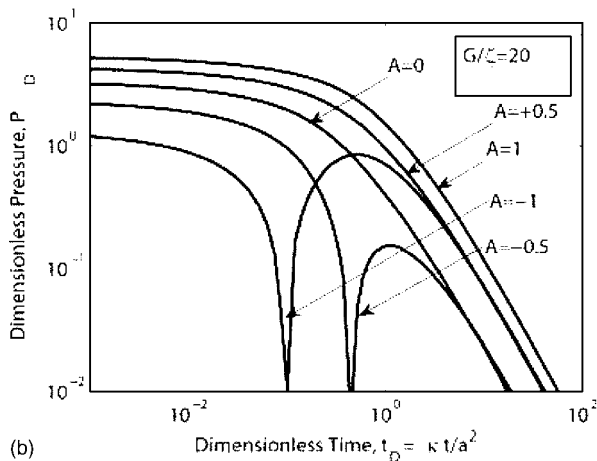
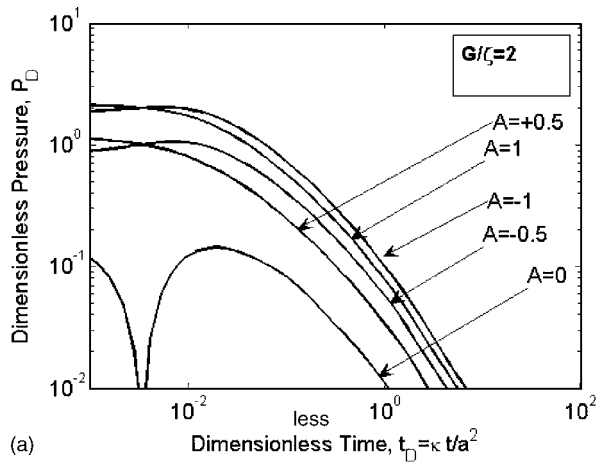


Fig. 5. Dissipation of dimensionless excess pore pressure with dimensionless time for initial pressure distributions for shear modulus to undrained strength ratios ( $G/\zeta$ ) of (a) 2; (b) 20; and (c) 200

drostatic, then again subhydrostatic, before asymptoting to the in situ magnitude. Typical responses are illustrated in Fig. 7. These are interpreted to result from dilatant soils that drive the initial tip-local steady pore pressures to be subhydrostatic. The arrest of penetration releases the loading on the rods that gives a pore pressure response dominated by local conditions at the cone face.



**Fig. 6.** Dissipation of dimensionless excess pore pressure with dimensionless time for initial pressure distributions for shear modulus to undrained strength ratios ( $G/\zeta$ ) of (a) 2, (b) 20, and (c) 200. This is a log-log replot of the semilog Fig. 5, with the subhydrostatic pore pressures (negative) plotted as their absolute positive magnitude.

As these disturbed tip-local pore pressures change, the influence of the zone, progressively more distant from the cone tip is felt, as pressure diffusion progresses. Ultimately, the influence of the distant zone of subhydrostatic pore pressures (Fig. 4) is felt, driving tip-local pressures below hydrostatic, before ultimately asymptoting to background pressures. It is this late-time subhydrostatic response that is observed both in the transient type curves

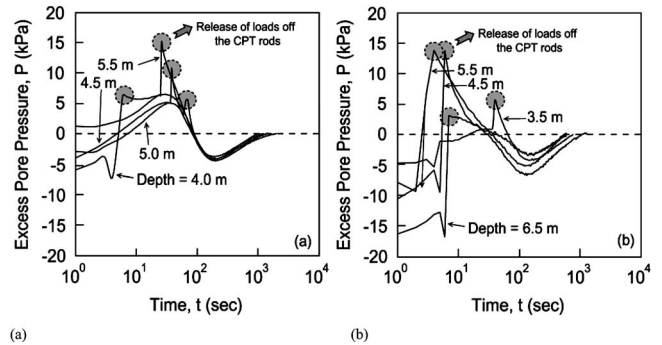


**Fig. 7.** Pore pressure records for uCPT dissipation tests in silty sand for soundings in two adjacent profiles. Pressures are recorded at the  $u_2$  location on the piezocone.

(Fig. 5), and the field observations that is used to backcalculate mechanical and transport properties from the dissipation response. These are used to determine the shear modulus to undrained strength ratio ( $G/\zeta$ ), undrained strength ( $\zeta$ ), and consolidation coefficient ( $\kappa$ ) from the field pore pressure dissipation data. These investigations are documented in the following.

### Typical Dissipation Data

Pore pressure dissipation records are evaluated for the shallow Milan, Mich. soundings in silty sand. The deposit is underlain by clay at a depth of  $\sim 6.5$  m with the water table present at  $\sim 1.7$  m below the ground surface. uCPT dissipation tests were conducted in two sounding profiles at depths of 4, 4.5, 5, and 5.5 m and 3.5, 4.5, 5.5, and 6.5 m below surface, in respective profiles. The pore pressures recorded at the  $u_2$  location are reported in Fig. 7. Two different types of responses of the excess pore pressure are apparent. The predominant response is where the initial excess pore pressure is subhydrostatic, but increases following the arrest of penetration, before dipping below hydrostatic on the way to equilibrium. The release of load from the CPT rod string causes a jump in the pore pressure. Suppressing the loss of load on the rods makes no significant change in the observed pressure response. The second type of response is where the initial pore pressure is suprahydrostatic (apparent in only one record at a depth of 5.5 m), but then follows the other curves noted previously. For both observed types of response, the time to the peak suprahydrostatic pressure, and to the ultimate trough in the subhydrostatic pressure are similar. This coherence in the observed pressure signal (Fig. 7) suggests that we are observing a characteristic of the system response, rather than an artifact of unloading resulting from the test. The peak in positive pressure occurs in the interval 10–20 s, and the peak in negative pressure in the range 100–200 s. The mechanisms responsible for this unusual pressure-dissipation response are examined in the following.

### Systematic Fitting of Type Curves

To enable representation of these pore pressures in log-pressure versus log-time space, the records of Fig. 7 are recast as the absolute magnitude of excess pressure as shown in Figs. 8 and 9. This transformation merely replots the semi-log plot as a log-log plot—as the subhydrostatic (negative) excess pressures cannot be represented on a log-scale, all negative pressures are plotted as their positive absolute magnitude. Importantly, the width of the pulse representing the negative pressure portion of the response is

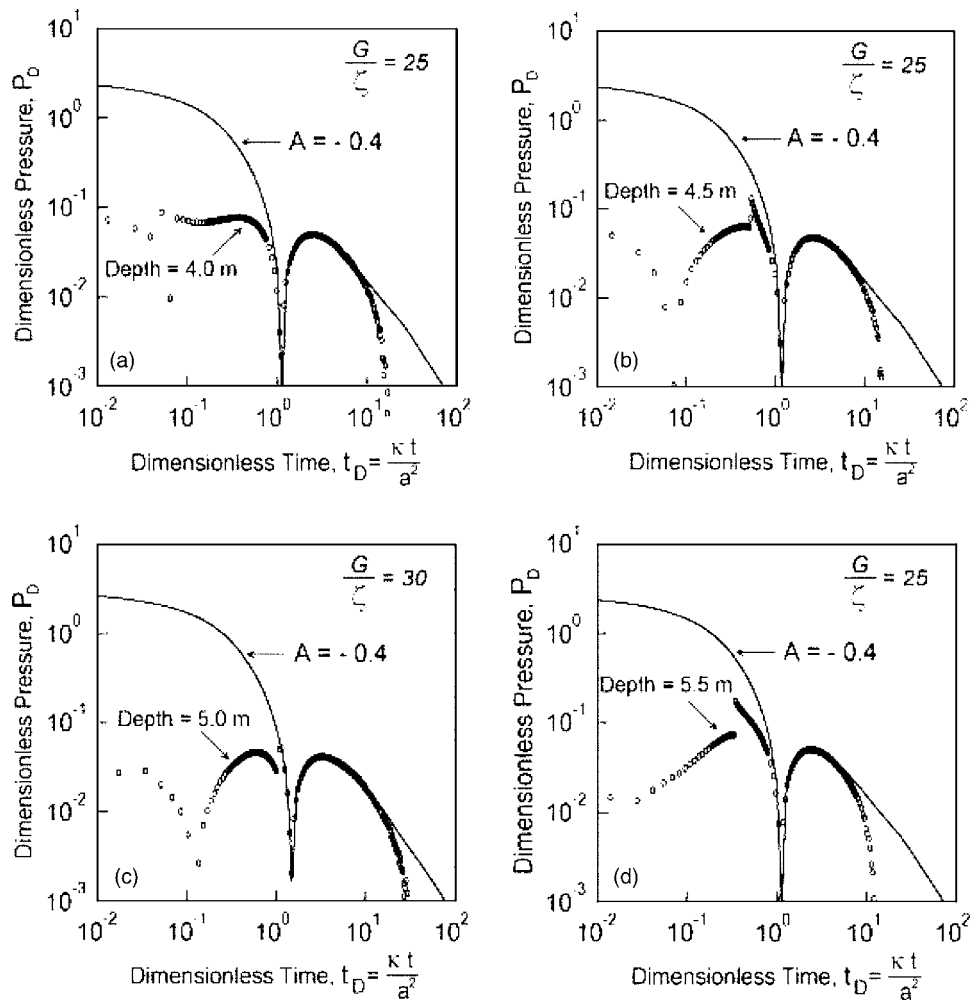


**Fig. 8.** Pressure dissipation data of Fig. 7 are shown (open circles) on the log-log type curves (solid line) of Fig. 6. The four dissipation tests are from Fig. 6.

indicative of the magnitude of the pore pressure factor  $A_f$ . For these particular data, a fit is not feasible for shear modulus to strength ratios  $G/\zeta$  of 2 or 200. However, the data are congruent with the type curves for  $G/\zeta=25-30$ , with  $A_f$  in the range from  $-0.4$  to  $-1.0$ . These data directly overprint the type curves for the late-time data, as shown in Figs. 8(a) and 9(d). Although the late-time match is excellent, the early-time data are not so well accommodated by this proposed model. This mismatch is magnified by the log-log representation. As the early-time pressure response is generally indicative of near field processes, the tip-local mechanisms of local redistribution of stresses following penetration arrest are implicated. Rod unloading is not the reason, as similar pressure response results when the rod load is maintained, post arrest. Alternately, near-tip shearing or shearing at the probe shaft may have an undue influence in the near-field and initial response.

The type curves may be used to recover material properties by fitting with the data. The unique shape of the pressure response curves identifies  $A_f \sim -0.4$  to  $1.0$  and  $G/\zeta \sim 20-30$  as illustrated in the remarkably consistent form of Figs. 8 and 9. The undrained strength ( $\zeta$ ) may be independently evaluated by matching the peak dimensionless excess pressure [ $P_D = (p-p_0)/\zeta = 0.1-1$ ] with the field-measured peak excess negative pore pressure ( $p-p_0 = 7-10$  kPa) to yield  $\zeta = 10-100$  kPa. Correspondingly, the negative pressure peak (trough) occurs at  $t_D=1$  and corresponds to an

actual time of  $t=60-112$  s. From  $t_D = \kappa t/a^2$ , and for  $a=1.78 \times 10^{-2}$  m this yields a consolidation coefficient of  $\kappa=2.8 \times 10^{-6}-5.2 \times 10^{-6}$  m<sup>2</sup>/s ( $\sim 2.8-5.2$  mm<sup>2</sup>/s). As the matches are for  $G/\zeta \sim 25-30$ , these correspond to effective shear moduli in the range 0.18–3.1 MPa.

These large strain magnitudes of shear modulus correspond to a moderate-strain modulus of 50 MPa recovered from dilatometer tests, and a small-strain modulus of 150 MPa recovered from shear wave velocity measurements, as identified in Table 1. This increase in magnitude with a reduction in the level of disturbance is as expected. Magnitudes of undrained strength are also recovered from the dilatometer tests, and at 200–400 kPa, these are broadly congruent with the upper-range strengths recovered from the dissipation tests at depth (Table 1).

#### Data for Overconsolidated Clays

Dissipation histories for uCPT penetration in clays ranging in overconsolidation ratio from 1.4 to 26 are compared against the results of this model. The collected data (Burns and Mayne 1998), for the eight sites exhibit only monotonic pore pressure dissipation in the long term, and are readily fit to semilog representations of the dissipation response, illustrated in Fig. 10 for magnitudes of  $G/\zeta$  of 2, 20, and 200. Of these anticipated responses only that for  $G/\zeta=200$  is absent subhydrostatic pore pressures in the very

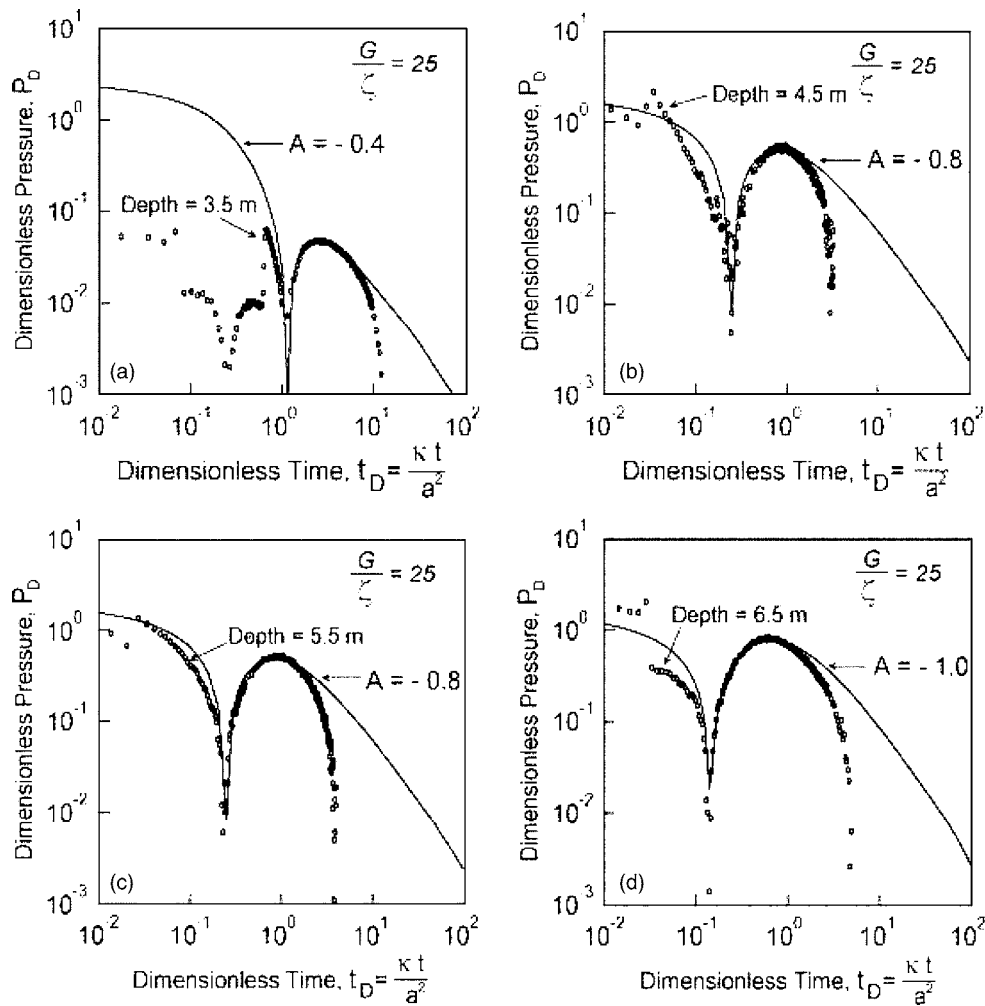


**Fig. 9.** Pressure dissipation data of Fig. 7 are shown (open circles) on the log-log type curves (solid line) of Fig. 6. The four dissipation tests are from Fig. 6.

long-term, close to the termination of the record. Correspondingly, the data are fitted to the response for  $G/\zeta=200$  shown in Fig. 10(c). The behavior for lightly overconsolidated clays and silts (OCR 1-1.4) is shown in Fig. 11(a), and for more heavily overconsolidated clays and silts (OCR 3.5-26) in Fig. 11(b). These resulting fits are for positive magnitudes of the Skempton parameter  $A$ , and enable magnitudes of consolidation coefficient to be determined from the matched  $t_{50}$  magnitude. As all dissipation type curves are similar, matching the observed  $t_{50}$  with the range of dimensionless  $t_{D50}$  magnitudes yields a range in consolidation coefficient magnitudes,  $\kappa$ . The nondimensional magnitudes

of  $t_{D50}$  range from  $2 \times 10^0 (A=1)$  to  $3 \times 10^{-1} (A=0)$ , and result in a bounded range of predicted magnitudes of consolidation coefficient. These predicted magnitudes are compared with laboratory measured magnitudes in Table 2 and show favorable agreement.

**Table 1.** Magnitudes of Shear Modulus, Consolidation Coefficient, and Shear Strength

Parameter	Dissipation test	DMT	Shear wave velocity
Undrained shear modulus, $G$ (MPa)	0.2–3	50	150
Consolidation coefficient, $\kappa$ ( $\text{mm}^2/\text{s}$ )	2.8–5.2	—	—
Undrained shear strength, $\zeta$ (kPa)	10–100	200–400	—

Note: Derived from dissipation and end bearing tests (this work), compared with independent evaluations from DMT and shear wave velocities.

## Conclusions

Anomalous pore pressure dissipation records, recovered from uCPT tests in silty sands are explained in terms of pore pressures developed as a result of undrained dilation in the soil within the tip process zone. Observed pore pressures are typically first subhydrostatic, transit to supra-hydrostatic, and then return to subhydrostatic before slowly equilibrating to the in situ pore pressure. The timing of these different peaks and troughs in the pore pressure response (Fig. 7) can be considered to reflect the distance of the affected zone from the recording location, i.e., the  $u_2$ -mounted transducer at the tip. The earliest events record the pore pressures diffusing from soil closest to the tip, and the latest events, telegraph the response from further away.

A model which represents the undrained pore pressure response of the soil to changes in applied spherical and deviatoric stresses is capable of replicating the intermediate- and late-time portion of this observed pore pressure response. If Skempton pore

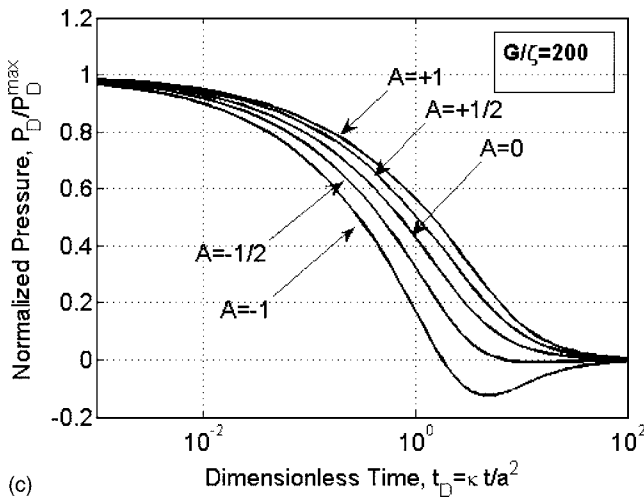
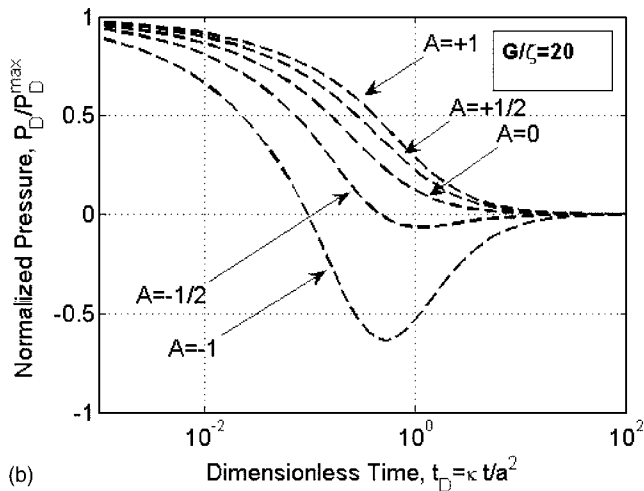
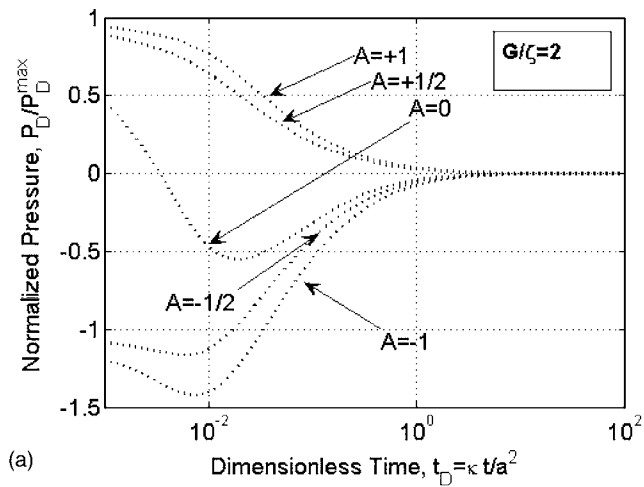


**Fig. 10.** Normalized pore pressure dissipation histories. Normalized relative to pressure at  $t_D=0$ . Distributions are for shear modulus to undrained strength ratios ( $G/\zeta$ ) of (a) 2, (b) 20, and (c) 200.

pressure parameters may be used to define the undrained response to spherical and deviatoric loads, then constitutive equations may be defined in terms of total stresses, and substituted into the spherically symmetric equilibrium conditions to determine the distribution of stresses and pore pressures which develop around an inflated spherical cavity. Importantly, the resulting total-stress

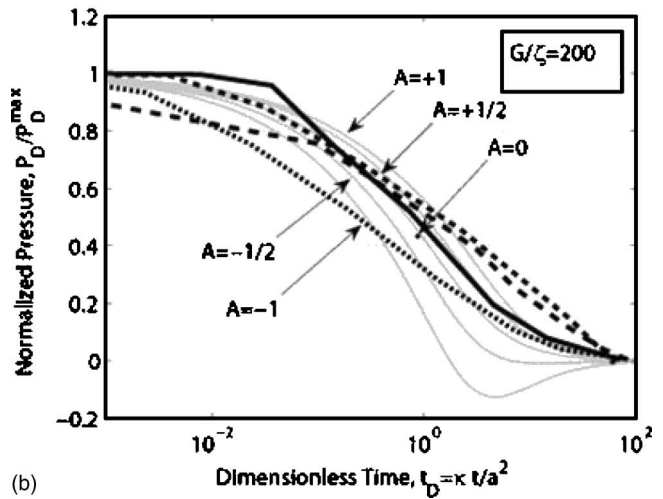
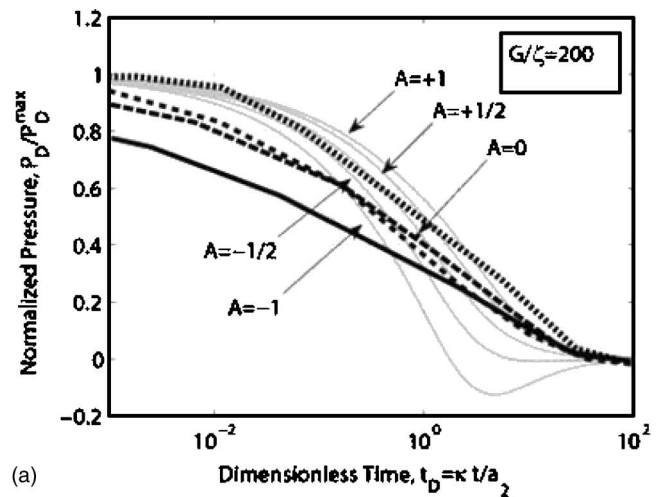


**Fig. 11.** Matches between dissipation histories recovered from this method, and monotonic pore pressure changes recorded in dilatant soils at sites worldwide. Citations for the original data are reported in Table 2 for (a) lightly and (b) heavily overconsolidated soils. Responses are for (a) Bothkennar, U.K. (solid); Drammen, Norway (long-dashed); McDonald Farm, B.C., Canada (short-dashed); St. Alban, Que., Canada (intermediate-dashed). (b) Amherst, Mass. (solid); Canon's Park, U.K. (long-dashed); St. Lawrence Seaway, N.Y. (short-dashed); and Taranto, Italy (intermediate-dashed). The type curves evaluated in this work are shown in gray.

constitutive equations are purely “cohesive,” enabling both the total stress and undrained pore pressure distribution to be straightforwardly determined. Within the failure zone, and as a consequence of this model, the induced mean stress is shown to decline log linearly with increasing radius from the cavity and potentially to become subhydrostatic remote from the cone face, whereas the deviatoric stress remains constant with radius. Induced pore pressures generated from these combined loading modes diminish with radius from the cavity wall, and may indeed become negative in the furthest extent of the failure zone. In the elastic region, beyond the failure zone, the undrained pore pressures are null. It is this resulting distribution of induced positive pore pressures close to the tip, and negative pore pressures at the outer extent of the failure zone, which results in both the first suprahydrostatic peak and the final subhydrostatic trough, observed in the field dissipation response. Not explained by this model, are the initial highly negative pore pressures recorded at very early times. These

**Table 2.** Comparison of Consolidation Coefficients Determined from this Method with Results of Dissipation Tests in Dilatant Materials (Data Adapted from Burns and Mayne 1998)

Site	Depth (m)	OCR	$t_{50}$ (s)	Laboratory	Dissipation	Comments	Reference
				measured	test measured		
				$c_v$ or $\kappa$ (mm <sup>2</sup> /s)	$c_v$ or $\kappa$ (this study) (mm <sup>2</sup> /s)		
Bothkennar, U.K.	12.0	1.4	1,000	0.32	0.13–0.48	Soft clay	Nash et al. 1992
Bothkennar, U.K.	12.0	1.4	1,000	0.08–0.13	0.13–0.48	Soft clay	Jacobs and Coutts 1992
Drammen, Norway	19.5	1.1	700	0.53–1.52	0.18–0.68	Marine clay	Lacasse and Lunne 1982
McDonald Farm, B.C., Canada	20.0	1.1	200	1.8–5.5	0.64–2.38	Lean insensitive clayey silt	Sully 1991
Saint Alban, Que., Canada	4.6	1.2	800	0.30	0.16–0.59	Sensitive clay	Roy et al. 1981
Amherst, Mass.	3.0	7.0	200	0.07–0.10	0.64–2.38	Crust of soft clay	DeGroot and Lutenegeger 1994; Lally 1993
Canon's Park, U.K.	5.7	14.0	9,000	0.01–0.03	0.12–0.43	102 mm pile in London Clay	Jardine and Bond 1989
St. Lawrence Seaway, N.Y.	6.1	3.5	600	0.25–0.80	0.21–0.79	Crust of soft clay	Lutenegeger and Kabir 1987
Taranto, Italy	9.0	26.0	1,000	0.10–0.25	0.13–0.48	Cemented clay	Battaglio et al. 1986; Bruzzi et al. 1987

are suggested to result from intense tip-local shearing, that is not accommodated in the simple representation of penetrometer advance as an expanding cavity (Burns and Mayne 1998).

In addition to explaining the general form of the pressure response, the analysis allows important parameters representing the mechanical and transport properties of the soil to be determined directly from the dissipation response. The parameters of shear modulus and undrained shear strength, accommodated in the analysis, are independently confirmed by measurements using the dilatometer test and through measurements of shear wave velocity. These independent measurements of modulus and strength are similar to the magnitudes recovered from the dissipation tests, but show a usual inverse trend in increasing modulus with a decrease in measurement strain. Although developed to represent observed responses in dilatant cohesionless soils, viz. silts, the model is also capable of replicating observed response in overconsolidated clays. Comparison with a series of dissipation tests, conducted worldwide, illustrate the correspondence of the type curves with observed response, and the corresponding ability to recover consolidation coefficients which are congruent with laboratory measured magnitudes, noted in Table 2. This congruence is perhaps not surprising, as these materials are already principally cohesive, and representing the mechanical response as one of cavity expansion in an effectively cohesive material is physically appropriate. This is not the case for materials with a higher frictional component within their strength, such as silts, which, perhaps surprisingly, may also be accommodated by the procedure developed in this work.

## Acknowledgments

This work is a result of partial support from the National Science Foundation under Grant No. CMS-04090002. This support is gratefully acknowledged. The writers also thank London Aggregates of Milan, MI, for site access, and Youngsub Jung and Jan Pantolin for onsite assistance.

## References

- Auxt, J. A., and Wright, D. (1995). "Environmental site characterization in the United States using the cone penetrometer." *Proc., CPT'95*, 387–392.
- Baligh, M. M. (1985). "Strain path method." *J. Geotech. Engrg.*, 111(9), 1108–1136.
- Baligh, M. M., and Levadoux, J. N. (1986). "Consolidation after undrained piezocone penetration. II: Interpretation." *J. Geotech. Engrg.*, 112(7), 727–745.
- Battaglio, M., Bruzzi, D., Jamiolkowski, M., and Lancellotta, R. (1986). "Interpretation of CPTs and CPTUs: Undrained penetration of saturated clays." *Proc., 4th Int. Geotechnical Seminar, Field Instrumentation and In Situ Measurements*, Singapore, 129–156.
- Battaglio, M., Jamiolkowski, M., Lancellotta, R., and Maniscalco, R. (1981). "Piezometer probe test in cohesive deposits." *Int. Conf. on Numerical Methods in Geomechanics*.
- Bruzzi, D., and Battaglio, M. (1987). "Pore pressure measurements during cone penetration tests." *I quaderni dell'ISMES (Experimental Institute for Models and Structures)*, Milan, Italy.
- Burns, S. E., and Mayne, P. W. (1998). "Monotonic and dilatatory pressure decay during piezocone tests in clay." *Can. Geotech. J.*, 35(6), 1063–1073.
- Campanella, R. G., and Robertson, P. K. (1988). "Current status of the piezocone test." *Penetration Testing 1988*, Orlando, Fla., 93–116.
- Chiang, C. Y., Loos, K. R., and Klopp, R. A. (1992). "Field determination of geological/chemical properties of an aquifer by cone penetrometry and head-space analysis." *Ground Water*, 30(3), 428–436.
- Cividini, A., and Gioda, G. (1988). "A simplified analysis of pile penetration." *Proc., 6th Int. Conf. on Numerical Methods in Geomechanics*, 1043–1049.
- Danziger, F. A. B., Almeida, M. S. S., and Sills, G. C. (1997). "The significance of the strain path analysis in the interpretation of piezocone dissipation data." *Geotechnique*, 47(5), 901–914.
- DeGroot, D. J., and Lutenegeger, A. J. (1994). "A comparison between field and laboratory measurements of hydraulic conductivity in a varved clay." *Hydraulic Conductivity and Waste Containment Transport in Soil*, 300–317.
- Douglas, B. J., and Olsen, R. S. (1981). "Soil classification using electric cone penetrometer." *Symp. on cone penetration testing and experience*, St. Louis, 209–227.
- Elsworth, D. (1991). "Dislocation analysis of penetration in saturated porous media." *J. Eng. Mech.*, 117(2), 391–408.
- Elsworth, D. (1993). "Analysis of piezocone dissipation data using dislo-

- cation methods." *J. Geotech. Engrg.*, 119(10), 1601–1623.
- Elsworth, D. (1998). "Indentation of a sharp penetrometer in a poroelastic medium." *Int. J. Solids Struct.*, 35(34–35), 4895–4904.
- Elsworth, D., and Lee, D. S. (2005). "Permeability determination from on-the-fly piezocone sounding." *J. Geotech. Geoenviron. Eng.*, 131(5), 643–653.
- Elsworth, D., and Lee, D. S. (2006). "Limits in determining permeability from on-the-fly uCPT soundings." *Geotechnique*, in review.
- Gribb, M. M., Simunek, J., and Leonard, M. F. (1998). "Development of cone penetrometer method to determine soil hydraulic properties." *J. Geotech. Geoenviron. Eng.*, 124(9), 820–829.
- Hill, R. (1983). *The mathematical theory of plasticity*, Clarendon, Oxford, New York.
- Hryciw, R. D., Shin, S., and Ghalib, A. M. (2003). "High resolution site characterization by visCPT with application to hydrogeology." *Proc., 12th Panamerican Conf. on Soil Mechanics*, Boston, 293–298.
- Jacobs, P. A., and Coutts, J. S. (1992). "A comparison of electric piezocone tips at the Bothkennar test site." *Geotechnique*, 42(2), 369–375.
- Jardine, R. J., and Bond, A. J. (1989). "Behaviour of displacement piles in heavily overconsolidated clay." *12th Int. Conf. Soil Mechanics and Foundation Engineering*, Rio de Janeiro, 1147–1151.
- Kiousis, P. D., and Voyiadjis, G. Z. (1985). "Lagrangian continuum theory for saturated porous media." *J. Eng. Mech.*, 111(10), 1277–1288.
- Konrad, J. M., and Frechette, P. (1995). "The piezocone-permeameter probe: A promising tool." *Proc., Geoenvironmental 2000, Characterization, Containment, Remediation and Performance Environmental Geotechnics, GSP*, 123–137.
- Kurup, P. U., Voyiadjis, G. Z., and Tumay, M. T. (1994). "Calibration chamber studies of piezocone tests in cohesive soils." *J. Geotech. Engrg.*, 120(1), 81–107.
- Lacasse, S., and Lunne, T. (1982). "Penetration tests in two Norwegian clays." *2nd European Symp. on Penetration Testing*, Amsterdam, The Netherlands, 661–669.
- Lally, M. J. (1993). "A field and laboratory investigation of geotechnical properties for design of a seasonal heat storage facility." Univ. of Massachusetts, Amherst, Mass.
- Levadoux, J. N., and Baligh, M. M. (1986). "Consolidation after undrained piezocone penetration. I: Prediction." *J. Geotech. Engrg.*, 112(7), 707–726.
- Lowry, B. (1998). "Cone permeameter in-situ permeability measurements with direct push techniques." Science and Engineering Associates, Inc.
- Lunne, T., Robertson, P. K., and Powell, J. J. M. (1997). *Cone penetration testing in geotechnical practice*, Blackie Academic Publishing.
- Lutenegger, A. J., and Kabir, M. J. (1987). "Pore pressures generated by two penetrometers in clays." *Rep. No. 87-2*, Dept. of Civil Engineering, Clarkson Univ., Potsdam, N.Y.
- Manassero, M. (1994). "Hydraulic conductivity assessment of slurry wall using piezocone test." *J. Geotech. Engrg.*, 120(10), 1725–1746.
- Mitchell, J. K., and Brandon, T. L. (1998). "Analysis and use of CPT in earthquake and environmental engineering." *Proc., Conf. on Geotechnical Site Characterization*, P. K. Robertson, and P. W. Mayne, eds., Atlanta, 69–96.
- Nash, D. F. T., Powell, J. J. M., and Lloyd, I. M. (1992). "Initial investigations of the soft clay test site at Bothkennar." *Geotechnique*, 42(2), 163–181.
- Randolph, M. F., and Wroth, C. P. (1979). "Analytical solution for the consolidation around a driven pile." *Int. J. Numer. Analyt. Meth. Geomech.*, 3(3), 217–229.
- Robertson, P. K., Campanella, R. G., Gillespie, D., and Greig, J. (1986). "Use of piezometer cone data." *Proc., Use of In Situ Tests in Geotechnical Engineering*, ASCE, Reston, Va., 1263–1280.
- Robertson, P. K., Sully, J. P., Woeller, D. J., Lunne, T., Powell, J. J. M., and Gillespie, D. G. (1992). "Estimating coefficient of consolidation from piezocone tests." *Can. Geotech. J.*, 29(4), 539–550.
- Roy, M., Blanchet, R., Tavenas, F., and Larochelle, P. (1981). "Behavior of a sensitive clay during pile driving." *Can. Geotech. J.*, 18(1), 67–85.
- Scaturro, D. M., and Wissowson, M. A. (1997). "Experimental evaluation of a drive-point ground-water sampler for hydraulic conductivity measurement." *Ground Water*, 35(4), 713–720.
- Schmertmann, J. H. (1978). "Guidelines for cone penetration test: Performance and design." *Technical Report, Federal Highway Administration, FHWA-TS-78-209*, FHWA, Washington, D.C.
- Skempton, A. W. (1954). "The pore pressure coefficients A and B." *Geotechnique*, 4, 143–147.
- Smythe, J. M., Bedient, P. B., Klopp, R. A., and Chiang, C. Y. (1989). "An advanced technology for the in situ measurement of heterogeneous aquifers." *Proc., Conf. on New Field Techniques in Quantifying the Physical and Chemical Properties of Heterogeneous Aquifers*, 605–628.
- Sully, J. P. (1991). "Measurement of in situ lateral stress during full-displacement penetration tests." Ph.D. thesis, Univ. of British Columbia, Vancouver, B.C., Canada.
- Teh, C., and Houlsby, G. (1991). "An analytical study of the cone penetration test in clay." *Geotechnique*, 41, 17–34.
- Torstensson, B. A. (1977). "The pore pressure probe." *Nordiske Geotekniske Mote*, Oslo, Norway, 34, 1–15.
- Van den Berg, V. D. (1994). "Analysis of soil penetration." Ph.D. thesis, Delft University, Delft, The Netherlands.
- Vesic, A. S. (1972). "Expansion of cavities in infinite soil mass." *J. Soil Mech. and Found. Div.*, 98(3), 265–290.
- Voyiadjis, G. Z., and Abu-Farsakh, M. Y. (1997). "Coupled theory of mixtures for clayey soils." *Comput. Geotech.*, 20(3/4), 195–222.
- Voyiadjis, G. Z., and Song, C. R. (2000). "Finite strain, anisotropic modified cam clay model with plastic spin. II: Application to piezocone test." *J. Eng. Mech.*, 126(10), 1020–1026.
- Voyiadjis, G. Z., and Song, C. R. (2003). "Determination of hydraulic conductivity using piezocone penetration test." *Int. J. Geomech.*, 3(3/4), 217–224.